Available online at www.sciencedirect.com
SCIENCE DIRECT®
ELSEVIER
International Journal of Solids and Structures 43 (2006) 1201–1223
INTERNATIONAL JOURNAL OF SOLIDS and STRUCTURES
www.elsevier.com/locate/ijsolstr

Energy release rate and mode partition for interlaminar crack in circular laminated beams

Domenico Bruno *, Rodolfo Carpino, Fabrizio Greco, Paolo Lonetti

Department of Structural Engineering, University of Calabria, Cosenza, Italy

Received 5 November 2004; received in revised form 16 March 2005
Available online 21 April 2005

Abstract

This work describes an improved technique for the analysis of interlaminar crack growth in laminated circular beams subjected to mixed-mode loading conditions. By adopting a multi-layer curved beam model and curved interface elements leads to model the structure as a succession of first-order shear deformable beams joined by adhesive interfaces. The interface containing the crack is simulated by means of a cracking linear interfacial constitutive law which provides normal and shear interlaminar stresses. At the perfectly bonded interfaces the connection between beam elements is imposed by the Lagrange multiplier method. The total energy release rate and its individual mode components are obtained when the stiffnesses, considered as penalty parameters, tend to infinity thus reproducing the results of the linear elastic fracture mechanics theory. Results are obtained by adopting an accurate numerical integration procedure able to deal with stress singularities at the crack tip. Comparisons with results available from literature obtained by using the elasticity theory and solid finite elements show that the model is able to capture accurately both the total and the individual mode components of energy release rate. Numerical examples demonstrate the capability of the proposed method to provide a complete description of the problem of mixed-mode crack growth in curved interfaces, which takes into account the influence of curvature and of transverse shear deformability.

Keywords: Layered structures; Interface; Delamination; Energy release rate; Mode partition; Curved laminated beam theory

* Corresponding author. Tel.: +39 984 496914; fax: +39 984 494045.
E-mail addresses: d.bruno@unical.it (D. Bruno), r.carpino@strutture.unical.it (R. Carpino), f.greco@unical.it (F. Greco), lonetti@unical.it (P. Lonetti).

0020-7683/$ - see front matter © 2005 Elsevier Ltd. All rights reserved.
doi:10.1016/j.ijsolstr.2005.03.054

1. Introduction

Laminated composite materials are extensively used in curved configurations in many civil and aerospace structural applications principally when high performances are required. Since layered composite structures exhibit relatively low interlaminar strengths, interface cracking or delamination is usually experienced when these structures are subjected to various loading conditions (e.g. transverse or axial loads, thermal loads and low velocity impacts). Curved composite structures, such as curved beams or shells, are more vulnerable to interface cracking than plane ones. In fact, due to geometrical curvature, high interlaminar tensile and shear stresses may develop leading to delamination failures (see, for instance, Kedward et al., 1989; Cui et al., 1996), as in the case of a cylindrically isotropic or anisotropic homogeneous curved beam where a pure bending induces interlaminar tensile stresses (e.g. Timoshenko, 1934; Lekhnitskii et al., 1968). The combination of material and geometrical discontinuities with curvature effects, in addition, increase the susceptibility to delamination (see for instance, McRobbie et al., 1995; Wisnom and Jones, 1995; Kaczmarek et al., 1998). Consequently several methodologies have been considered to diminish the tendency to interlaminar cracking in curved structures (Cox et al., 1996). The phenomenon of interface crack propagation in curved laminated structures may lead to a local or global failure and, therefore, must be accurately investigated.

Interface cracking in layered plates and beams have been analyzed by using both damage mechanics (see, for example, Allix and Corigliano, 1999; Camanho et al., 2003; Zou et al., 2003) and fracture mechanics concepts (see for example, Hutchinson and Suo, 1992; Raju, 1987; Zou et al., 2002, 2001; Wang and Qiao, 2004a,b; Bruno and Greco, 2001; Bruno et al., 2003). According to the former approach interface elements with softening constitutive laws are usually adopted between solid elements (Camanho et al., 2003; Zou et al., 2003) or beam/shell elements (Allix and Corigliano, 1999; Zou et al., 2003). In the latter approach, the total energy release rate and its individual mode components need to be evaluated in order to predict delamination growth. For general configurations energy release rates can be computed by using a very accurate mesh of solid finite elements and the virtual crack closure technique (Raju, 1987). For laminated beam/plate structures solid finite elements may require a large computational effort and it can be more efficient to use plate theory. Therefore the earlier delamination models based on classical plate theory, which are unable to unable to accurately predict the individual energy release rates, have been improved according to different methods. For example, the elasticity theory in conjunction with classical plate theory (Hutchinson and Suo, 1992) or with improved plate theory to capture the effect of shear deformation (Wang and Qiao, 2004a,b), has been efficiently adopted. Moreover, shear deformable sublaminates and the virtual crack closure technique have been used to obtain a reasonable approximation to the mode separation solution (Zou et al., 2001). Finally, interface models have been used in conjunction with a two-layer shear deformable laminate model to obtain a refined energy release rate computation (Bruno and Greco, 2001), or in combination with a multi-layer shear deformable laminate model to capture with reliability the three-dimensional nature of the mode partition problem (Bruno et al., 2003).

On the other hand, few analyses have been devoted to the analysis of interfacial cracking in curved layered structures especially with reference to the mode partition problem, which is a notable aspect for this kind of structures. In curved layered structures, in fact, due to strains and material coupling effects mixed mode conditions are induced more frequently than in the case of rectilinear structures and the decomposition of the total energy release rate into its mode components becomes a necessary task, due to the mode-mix dependency of interface toughness (see, for instance, Reeder, 1993). The analyses of interlaminar cracking in curved interfaces have been developed mainly by using 2D or 3D solid finite elements and fracture mechanics concepts (Kaczmarek et al., 1998; Münch and Ousset, 2002; Lu et al., 1994; Figiel and Kamiński, 2003). A numerical delamination model has been developed for delamination growth in three-dimensional curved interfaces in (Münch and Ousset, 2002) by using 3D solid finite elements. Plane stress quarter-point finite elements have been adopted in (Lu et al., 1994) to analyze a delaminated curved

beam of a cylindrical orthotropic material. The total energy release rate has been calculated by the local stress field by using solid plane stress finite elements in (Figiel and Kamiński, 2003) to analyze fatigue delamination. Finally, the strain energy release rates for edge delamination in laminated fiber-reinforced beams loaded in bending, have been computed in (Kaczmarek et al., 1998) by using the virtual crack-closure technique and 3D solid finite elements. However, the simulation of the singular near-tip stresses requires a very dense mesh of solid finite elements with the use of higher order or singular finite elements which may lead to a large computational effort. Therefore, models based on plate theory which can be more convenient if used in place of the continuum approach, should be investigated. Unfortunately, as shown in (Lu et al., 1994) the classical thin curved beam theory is able to capture only the main characteristics of the solution but is inaccurate for thicker beams. Moreover the curved beam theory can be used only to compute the total energy release rate.

To this end, the aim of this paper is to extend the approach introduced in (Bruno et al., 2003) based on a refined plate theory, which has shown its efficiency for plane delamination problem in laminated plates, to the case of delamination of circular layered beams. The circular laminated beam is simulated by a succession of curved layers connected by interfaces. The combined effects of membrane, flexural and shear deformations are included by adopting a first order shear deformable curved beam theory for each layer. The interfaces, modeled as zero thickness layers, simulate the presence of an interfacial crack by means of a cracking constitutive law and ensure displacement continuity between layers in the uncracked regions. Two constraint methods has been incorporated into the interface models to improve the efficiency of the approach, namely, the penalty and Lagrange multipliers methods. The former, used in the delaminated interface, is adopted to recover interlaminar shear and normal stresses by using the stiffness parameters of the constitutive law as penalty coefficients, whose singularities leads to compute the total energy release rate and its individual mode I and II components. The latter is implemented to reduce the number of generalized displacement variables. The analysis is carried out solving, by means of an accurate numerical integration scheme, the boundary value problem obtained by a variational formulation. Results are obtained for curved beams loaded by end forces and in pure bending in order to show the influence of shear deformation and of curvature and compared to those obtained by using solid finite element models. Both the case of a homogeneous isotropic and cylindrical orthotropic curved beam are considered in numerical examples.

2. Curved laminated beam with an interfacial crack

The plane crack problem shown in Fig. 1 is considered where a through-the-width crack is located along the curved interface between the upper sub-laminate of thickness h_2 and the lower sub-laminate of thickness h_1. A global polar co-ordinate system is introduced where r is the radial direction and θ the circumferential direction. The crack is located at $r = R_D$. The circumferential dimension of the laminated beam is equal to θ_T and the dimension of interfacial crack is equal to θ_D. Both the two sub-laminates are assumed to be composed of plies made of homogeneous cylindrically orthotropic linear elastic materials. This problem is modeled here as a succession of curved beam elements joined by interfaces in the thickness direction. The number of curved beam elements is n_l for the lower and n_u for the upper sub-laminate. The first curved beam element is the lowest one. A local right-handed curvilinear co-ordinate system x_i, z_i is placed for each beam element on the beam mid-axis as shown in Fig. 2, being related to the global polar co-ordinate system by the following transformation laws:

$$\begin{cases} x_i = R_i\theta, \\ z_i = R_i - r, \end{cases} \tag{1}$$

where R_i is the radius of curvature of the generic beam element.

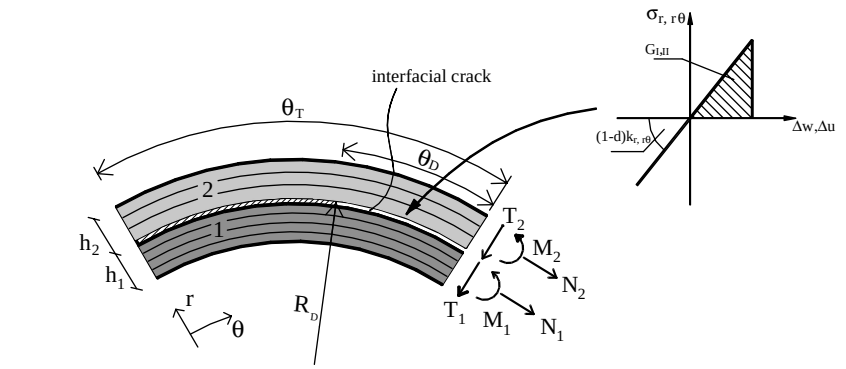

Fig. 1. Schematic illustration of the curved delaminated beam subjected to general loadings.

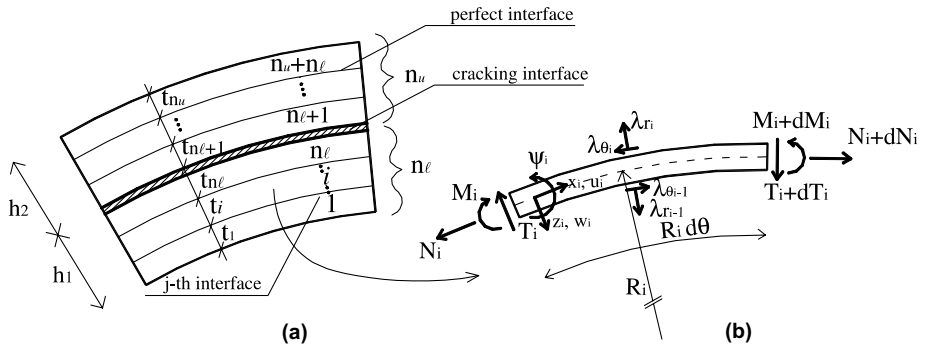

Fig. 2. Assembly of beam elements and interfaces (a) and forces on a small beam element (b).

The thickness of the ith curved-beam element is denoted by t_i. Each curved beam element may represent a single ply or an assembly of plies. Therefore material coupling is incorporated in constitutive relations. As a consequence, in a typical curved beam element the resultant axial force N_i, moment M_i and transverse shear force T_i for unit width, can be related to the tangential strain ε_i, curvature κ_i and transverse shear strain γ_i by means of the classical extensional A_i, bending–extensional coupling B_i and bending stiffnesses D_i (see for example Jones, 1975) in the following form:

$$\begin{Bmatrix} N_i \\ M_i \\ T_i \end{Bmatrix} = \begin{bmatrix} A_i & B_i & 0 \\ B_i & D_i & 0 \\ 0 & 0 & H_i \end{bmatrix} \begin{Bmatrix} \varepsilon_i \\ \kappa_i \\ \gamma_i \end{Bmatrix}, \tag{2}$$

where the stiffnesses can be expressed in the following form:

$$(A_i, B_i, D_i) = \int_{-t_i/2}^{t_i/2} \overline{E}_i(z_i)(1, z_i, z_i^2)\,\mathrm{d}z_i, \quad H_i = \int_{-t_i/2}^{t_i/2} fG_i(z_i)\,\mathrm{d}z_i, \tag{3}$$

where $\overline{E}_i$ is an equivalent longitudinal modulus, G_i is the transverse shear modulus, f is the shear correction factor chosen as 5/6 in this work, and v_{xyi} are the Poisson ratios of the beam i. For plane stress and plane strain assumptions in the y-direction $\overline{E}_i$ assumes the following expressions:

$$\overline{E}_i = \begin{cases} E_i & \text{(plane stress)}, \\ \dfrac{E_i}{1 - v_{xyi}v_{yxi}} & \text{(plane strain)}. \end{cases}$$

Since the coupling between bending and stretching is neglected and the classical definition for the stiffnesses is adopted, the constitutive law (2) is valid for small values of the thickness to curvature radius ratio (see Baldacci, 1983). However, it is worth noting that in the present model this hypothesis can be satisfied to the desired accuracy by introducing several beam elements into each sub-laminate. Moreover, as it will be shown in the following, introducing interface elements leads to capture both radial and tangential interlaminar stresses which develop in the curved beam due to curvature effects, which are neglected in classical curved beam theory.

At an arbitrary point of the beam element the displacements in the positive directions of the axis x, z are denoted respectively as $\bar{u}_i$ and $\bar{w}_i$, ψ_i denotes rotations of transverse sections about y-axis. The curved beam mechanical model accounts for flexural, extensional and transverse shear deformability in the plane of the curved beam. To this end, the laminated shell theory developed in (Reddy, 1982) which contains the first order shear deformation theory of flat plates as special cases, specialized to the case of curved beams is adopted. The displacements can be written as

$$\begin{aligned} \bar{u}_i(x_i, z_i) &= u_i(x_i) + z_i\psi_i(x_i), \\ \bar{w}_i(x_i, z_i) &= w_i(x_i), \end{aligned} \tag{4}$$

where $u_i(x_i)$ and $w_i(x_i)$ are respectively the tangential and radial displacements of the mid-axis of the i-th beam element. The strains in the curvilinear co-ordinate systems and in the global co-ordinate system respectively are:

$$\begin{cases} \varepsilon_i = \dfrac{\mathrm{d}u_i}{\mathrm{d}x_i} - \dfrac{w_i}{R_i} \\ \kappa_i = \dfrac{\mathrm{d}\psi_i}{\mathrm{d}x_i} \\ \gamma_i = \dfrac{\mathrm{d}w_i}{\mathrm{d}x_i} + \dfrac{u_i}{R_i} + \psi_i \end{cases} \qquad \begin{cases} \varepsilon_i = \dfrac{u_i'}{R_i} - \dfrac{w_i}{R_i}, \\ \kappa_i = \dfrac{\psi_i'}{R_i}, \\ \gamma_i = \dfrac{w_i'}{R_i} + \dfrac{u_i}{R_i} + \psi_i, \end{cases} \tag{5}$$

where prime denotes the derivative with respect to θ. Note that Eq. $(5)_2$ are obtained from Eq. $(5)_1$ by virtue of the co-ordinate transformation laws expressed in Eq. (1).

The generic jth interface between the jth and the $j+1$th beam element inside each sub-laminates is introduced to impose the following displacement continuity conditions:

$$\Delta\bar{u}_j = 0, \quad \Delta w_j = 0, \tag{6}$$

where

$$\begin{cases} \Delta\bar{u}_j = u_j - \frac{t_j}{2}\psi_j - u_{j+1} - \frac{t_{j+1}}{2}\psi_{j+1} = 0 \\ \Delta w_j = w_j - w_{j+1} = 0 \end{cases} \qquad j = 1, \ldots, n_u + n_l - 1. \tag{7}$$

The constraint conditions (6) are implemented by using the Lagrange multiplier method. On the other hand the interface containing the delamination, which is the n_l-th interface, bonds perfectly the beam elements n_l and n_{l+1} in the uncracked region thus ensuring continuity of circumferential and radial displacements, whereas in the cracked region sub-laminates may deform independently. A linear elastic interfacial constitutive law is therefore introduced which involves two stiffness parameters, namely k_r and $k_{r\theta}$, corresponding to penalty parameters. Denoting the interlaminar normal and circumferential stresses by σ_r and $\sigma_{r\theta}$, respectively, the constitutive relation (see Fig. 1) assumes the following expression:

$$\sigma_r = (1-d)k_r\Delta w_{n_l}, \quad \sigma_{r\theta} = (1-d)k_{r\theta}\Delta\bar{u}_{n_l}, \tag{8}$$

where the relative interface displacements $\Delta\bar{u}_{n_l}$ and Δw_{n_l}, are:

$$\Delta w_{n_l} = w_{n_l} - w_{n_l+1}, \quad \Delta\bar{u}_{n_l} = u_{n_l} - \frac{t_{n_l}}{2}\psi_{n_l} - u_{n_l+1} - \frac{t_{n_l+1}}{2}\psi_{n_l+1},$$

and d is a fracture variable, taking the value 1 value for no adhesion, namely for $\theta_T - \theta_D\theta \leqslant \theta_T$, and the value 0 for perfect adhesion, namely for $0 \leqslant \theta \leqslant \theta_T - \theta_D$. The fracture variable simulates interfacial crack by reducing to zero interface stiffnesses.

Applying the virtual crack closure concept (for details see Bruno and Greco, 2001) in terms of stresses and relative displacements evaluated in the n_lth interface layer leads to the following direct mode decomposition:

$$G_I = \lim_{k_{r\theta},k_r\to\infty} \frac{1}{2} k_r \Delta w_{n_l}^2, \quad G_{II} = \lim_{k_{r\theta},k_r\to\infty} \frac{1}{2} k_{r\theta} \Delta \bar{u}_{n_l}^2, \tag{9}$$

where subscript I, II denotes modes I and II components of energy release rate, Δw_{n_l} and $\Delta \bar{u}_{n_l}$ are evaluated at the interfacial crack tip and an opening displacement $\Delta w_{n_l} \geqslant 0$ is assumed. Contact between cracked sublaminates is not taken into account here. The interface constitutive law Eq. (8) can be opportunely extended in order to prevent interpenetration between delaminated sub-laminates in the delaminated region. For example, an interface constitutive law similar to that introduced in Eq. (3) by (Bruno et al., 2003) could be used, which adopts a unilateral frictionless contact interface along the delaminated region, characterized by a zero stiffness for opening relative displacements ($\Delta w \geqslant 0$) and a very high positive stiffness for closing relative displacements ($\Delta w < 0$), thus restricting sub-laminate overlapping and simulating contact condition.

Since the above described curved beam model implies continuity in tangential and radial displacements along the uncracked regions of the interfaces whereas discontinuity in rotations is allowed across interfaces, an accurate kinematical description is obtained which is able to capture adequately shear effects. Moreover, the introduction of interfaces provides a model to evaluate interlaminar radial and circumferential stresses which are of notable importance for curved beam in bending in order to predict accurately the interfacial cracking.

3. Variational formulation of the problem

Assuming a quasi-static interface crack growth, the relative interface displacements $\Delta \bar{u}_{n_l}$ and Δw_{n_l} must be computed from an equilibrium solution of the system.

The equilibrium equations for the structural system are derived here through the stationarity condition of the modified total potential energy functional for unit width Π_k, which includes interface displacement continuity and adhesion constraints by means of Lagrangian and penalty functionals, respectively.

The modified total potential energy functional for unit width of the beam, can be expressed as follows:

$$\Pi_k(u_i, w_i, \psi_i) = U + I + L - W, \tag{10}$$

where U is the strain energy of the whole multi-layer model of the curved beam, I is the strain energy of the cracking interface representing the penalty functional, L denotes the Lagrange functional constraint for adhesion between uncracked beam elements and W is the work of the external loads.

The strain energy is obtained by assembling contributes from each curved-beam element

$$U = \sum_{i=1}^{n_u+n_l} \int_0^{\theta_T} [\Phi_i(u_i, w_i, \psi_i)] R_i \, d\theta, \tag{11}$$

where Φ_i is the strain energy density of the ith beam element

$$\Phi_i(u_i, w_i, \psi_i) = \frac{1}{2}(N_i\varepsilon_i + T_i\gamma_i + M_i\kappa_i).$$

The strain energy of the interface containing the interface crack assumes the form

$$I = \int_0^{\theta_T} \Lambda R_D \, d\theta, \quad \Lambda = \frac{1}{2}(\bar{k}_r \Delta w_{n_l}^2 + \bar{k}_{r\theta} \Delta \bar{u}_{n_l}^2), \tag{12}$$

where

$$\bar{k}_r = (1-d)k_r, \quad \bar{k}_{r\theta} = (1-d)k_{r\theta}.$$

On the other hand, the Lagrange functional related to interface displacement continuity between adjoining beam elements can be expressed as

$$L = \sum_{j=1}^{n_l+n_u-1} \int_0^{\theta_T} [\lambda_{uj}\Delta\bar{u}_j + \lambda_{wj}\Delta w_j]\overline{R}_j \,\mathrm{d}\theta \quad j \neq n_l, \tag{13}$$

where $\Delta\bar{u}_j$ and Δw_j denote relative displacements at the jth interface between the jth and the $j+1$th beam element evaluated as expressed by Eq. (7) and

$$\overline{R}_j = R_j + \frac{t_j}{2}.$$

Moreover, λ_{uj} and λ_{wj} are the Lagrange multipliers representing interlaminar stresses at the jth interface.

The equilibrium equations are derived from the first variation of (10)

$$\begin{aligned} &\delta\Pi_k(u_i, w_i, \psi_i, \lambda_{uj}, \lambda_{wj}, k_r, k_{r\theta}) = 0, \\ &\forall\{\delta u_i, \delta w_i, \delta\psi_i, \delta\lambda_{uj}, \delta\lambda_{wj}\}, \quad i = 1, \ldots, n_l + n_u, \;\; j = 1, \ldots, \;\; n_l + n_u - 1, \;\; j \neq n_l, \end{aligned} \tag{14}$$

valid for every kinematically admissible displacements, which gives the following expression:

$$\begin{aligned} \delta\Pi_k = &\sum_{i=1}^{n_l+n_u} \int_0^{\theta_T} \left[N_i\left(\frac{\delta u_i'}{R_i} - \frac{\delta w_i}{R_i}\right) + T_i\left(\frac{\delta w_i'}{R_i} + \frac{\delta u_i}{R_i} + \delta\psi_i\right) + M_i\left(\frac{\delta\psi_i'}{R_i}\right)\right] R_i \,\mathrm{d}\theta \\ &+ \int_0^{\theta_T} \left[\bar{k}_{r\theta}\Delta\bar{u}_{n_l}\delta\Delta u_{n_l} + \bar{k}_r\Delta w_{n_l}\delta\Delta w_{n_l}\right] R_D \,\mathrm{d}\theta \\ &+ \sum_{j=1}^{n_l-1} \int_0^{\theta_T} \left[\lambda_{uj}\delta\Delta\bar{u}_j + \lambda_{wj}\delta\Delta w_j + \Delta\bar{u}_j\delta\lambda_{uj} + \Delta w_j\delta\lambda_{wj}\right]\overline{R}_j \,\mathrm{d}\theta \\ &+ \sum_{j=n_l+1}^{n_l+n_u-1} \int_0^{\theta_T} \left[\lambda_{uj}\delta\Delta\bar{u}_j + \lambda_{wj}\delta\Delta w_j + \Delta\bar{u}_j\delta\lambda u_j + \Delta w_j\delta\lambda w_j\right]\overline{R}_j \,\mathrm{d}\theta \\ &- \sum_{i=1}^{n_l+n_u} \left[\overline{N}_i\delta u_i + \overline{T}_i\delta w_i + \overline{M}_i\delta\psi_i\right]_0^{\theta_T} = 0, \end{aligned}$$

where the overbarred N_j, T_j, M_j denotes the applied forces.

The variation with respect to Lagrange multipliers furnishes the following equations expressing displacement continuity requirements at interfaces between plate elements:

$$\begin{cases} \Delta\bar{u}_j = 0 \\ \Delta w_j = 0 \end{cases} \quad j = 1, \ldots, \;\; n_u + n_l - 1, \;\; j \neq n_l, \tag{15}$$

which by using Eq. (7) result in

$$\begin{cases} w_i = w_{n_l} \quad i = 1, \ldots, n_l - 1, \\ w_i = w_{n_l+1} \quad i = n_l + 2, \ldots, n_l + n_u, \end{cases}$$

$$\begin{cases} u_i = u_{n_l} + \frac{t_{n_l}}{2}\psi_{n_l} + \sum_{k=j+1}^{n_l-1} t_k\psi_k + \frac{t_i}{2}\psi_i \quad i = 1, \ldots, n_l - 1, \\ u_i = u_{n_l+1} - \frac{t_{n_l+1}}{2}\psi_{n_l+1} - \sum_{k=n_l+2}^{i-1} t_k\psi_k - \frac{t_i}{2}\psi_i \quad i = n_l + 2, \ldots, n_l + n_u. \end{cases} \tag{16}$$

Using Eq. (16) leads to rewrite the differential problem in terms of only $n_l + n_u + 4$ displacement variables, which are assumed to be

$$w_{n_l}, w_{n_l+1}, u_{n_l}, u_{n_l+1}, \psi_i (i = 1, \ldots, n_1 + n_u). \tag{17}$$

Elimination of Lagrange multipliers leads to the following relations:

$$\begin{aligned}
&\lambda_{uj} = \sum_{k=1}^{j} \frac{N'_k}{\overline{R}_j} - \sum_{k=1}^{j} \frac{T_k}{\overline{R}_j}, \quad j = 1, \ldots, n_l - 1, \quad \lambda_{uj} = -\sum_{k=j+1}^{n_l+n_u} \frac{N'_k}{\overline{R}_j} + \sum_{k=j+1}^{n_l+n_u} \frac{T_k}{\overline{R}_j}, \quad j = n_l + 1, \ldots, n_l + n_u - 1, \\
&\lambda_{wj} = \sum_{k=1}^{j} \frac{N_k}{\overline{R}_j} + \sum_{k=1}^{j} \frac{T'_k}{\overline{R}_j}, \quad j = 1, \ldots, n_l - 1, \quad \lambda_{wj} = -\sum_{k=1}^{j} \frac{N_k}{\overline{R}_j} - \sum_{k=1}^{j} \frac{T'_k}{\overline{R}_j}, \quad j = n_l + 1, \ldots, n_l + n_u - 1.
\end{aligned} \tag{18}$$

Then, performing integration by parts gives the following equilibrium equations:

$$\begin{aligned}
&\sum_{i=1}^{n_l} [-N'_i + T_i] + \bar{k}_{r\theta} R_D \Delta \bar{u}_{n_l} = 0, \\
&\sum_{i=n_l+1}^{n_l+n_u} [-N'_i + T_i] - \bar{k}_{r\theta} R_D \Delta \bar{u}_{n_l} = 0,
\end{aligned} \tag{19}$$

which represent local equilibrium in the θ-direction for the lower and upper sub-laminate, respectively;

$$\begin{aligned}
&\sum_{j=1}^{n_l} [-N_j + T'_j] + \overline{k_r} \Delta w_{n_l} R_D = 0, \\
&\sum_{j=n_l+1}^{n_l+n_u} [-N_j + T'_j] - \overline{k_r} \Delta w_{n_l} R_D = 0,
\end{aligned} \tag{20}$$

which represent local equilibrium in the r-direction for the lower and upper multi-layered beam, respectively;

$$\begin{aligned}
&R_1 T_1 - M'_1 - \lambda_{u1} \frac{t_1}{2} \overline{R}_1 = 0, \\
&\ldots \\
&R_i T_i - M'_i - \lambda_{ui} \frac{t_i}{2} \overline{R}_i - \lambda_{ui-1} \frac{t_{i-1}}{2} \overline{R}_{i-1} = 0 \quad i = 2, \ldots, n_l - 1, \\
&\ldots \\
&R_{n_l} T_{n_l} - M'_{n_l} - \lambda_{un_l-1} \frac{t_{n_l-1}}{2} \overline{R}_{n_l-1} - R_D \bar{k}_{r\theta} \Delta \bar{u}_{n_l} \frac{t_{n_l}}{2} = 0, \\
&T_{n_l+1} R_{n_l+1} - M'_{n_l+1} - \lambda_{un_l+1} \frac{t_{n_l+1}}{2} \overline{R}_{n_l+1} - R_D \bar{k}_{r\theta} \Delta \bar{u}_{n_l} \frac{t_{n_l+1}}{2} = 0, \\
&\ldots \\
&R_i T_i - M'_i - \lambda_{ui} \frac{t_i}{2} \overline{R}_i - \lambda_{ui-1} \frac{t_{i-1}}{2} \overline{R}_{i-1} = 0 \quad i = n_l + 2, \ldots, n_l + n_u - 1, \\
&\ldots \\
&T_{n_l+n_u} R_{n_l+n_u} - M'_{n_l+n_u} - \lambda_{un_l+n_u-1} \frac{t_{n_l+n_u-1}}{2} \overline{R}_{n_l+n_u-1} = 0,
\end{aligned} \tag{21}$$

which represent local rotational equilibrium for each curved-beam element comprised in the lower and upper sublaminate, respectively. Eqs. (19)–(21) by using Eqs. (2)–(16) may be expressed in terms of the reduced set of displacement variables collected in Eq. (17). Moreover, integration by parts gives the boundary condition equations which are not detailed here for the sake of brevity.

4. Numerical studies and comparisons with classical FE models

In this section two sets of numerical calculations are presented. The first set is devoted to the analysis of a curved beam under bending containing an internal interfacial crack along its mid-axis, for which a solution obtained via finite elements of the plane stress elasticity problem can be found in (Lu et al., 1994). The second one is related to the analysis of edge interfacial crack in a curved layered beam loaded by edge transverse and axial forces. Both the case of homogeneous isotropic and cylindrically orthotropic materials are analyzed in the developed examples. Comparisons are made with numerical evaluations of energy release rates as a function of the interface crack length obtained using the virtual crack closure method and a classical 2D finite element model.

Results will evidence the ability of the proposed model to improve solutions obtained by using the classical beam-theory models providing a good approximation of the two-dimensional curved interfacial crack problem.

4.1. Numerical approximation of the curved interfacial crack problem

The boundary value problem governing the equilibrium of the delaminated curved composite structure subjected to applied forces can be reformulated as a non-linear system of first order ordinary differential equations subjected to boundary conditions at two-points. Non-linearities are lumped at the interface constitutive law level and arise as a consequence of the use of the fracture variable d. As a matter of fact, the interface constitutive law Eq. (8) is a piecewise continuous function of θ, since the effects of an interface crack are modeled by an abrupt drop of interface stiffnesses. The introduction of the fracture variable, although complicating the mathematical structure of the differential problem, leads to a notable reduction of the size of the differential problem since makes it possible to avoid the division of the integration domain $0 \leqslant \theta \leqslant \theta_T$ into two sub-domains (namely $0 \leqslant \theta \leqslant \theta_T - \theta_D$ and $\theta_T - \theta_D < \theta \leqslant \theta_T$). Actually, in the case when two adjoining domains are considered, the differential problem becomes linear, but the number of differential equations which must be solved are twice those of the case of a single domain and additional matching boundary conditions must taken into account at $\theta = \theta_T - \theta_D$.

The reformulated boundary value problem assumes the form

$$\boldsymbol{y}'_k(\theta) = \boldsymbol{g}_k(\boldsymbol{y}_k, \theta), \quad 0 \leqslant \theta \leqslant \theta_T, \tag{22}$$

where $\boldsymbol{y}$ is a vector collecting displacement unknowns and their derivatives:

$$y = \{u_{n_l}, u'_{n_l}, u_{n_l+1}, u'_{n_l+1}, w_{n_l}, w'_{n_l}, w_{n_l+1}, w'_{n_l+1}, \psi_1, \psi'_1, \ldots, \psi_{n_l+n_u}, \psi'_{n_l+n_u}\}^T, \tag{23}$$

and $\boldsymbol{g}$ is an opportune vector function describing the boundary value problem. In Eqs. (22) and (23) the prime denotes differentiation with respect to. The subscript k denotes explicit dependence of the solution $\boldsymbol{y}$ from the penalty parameters. Eq. (22) is subjected to the following two-point linear boundary conditions:

$$\boldsymbol{B}_0 \boldsymbol{y}_k(0) + \boldsymbol{B}_1 \boldsymbol{y}_k(1) = \boldsymbol{c}, \tag{24}$$

where $\boldsymbol{B}_0$ and $\boldsymbol{B}_1$ are opportune matrices containing the coefficients of boundary conditions and $\boldsymbol{c}$ is an opportune known vector depending on the applied forces.

The two-point boundary value problem for fixed values of the penalty parameters, has been solved by means of an iterative collocation method implemented in MATLAB® (The MathWorks Inc., 2000) which provides a C^1-continuous solution by using a cubic collocation polynomial on each subinterval of the mesh. Starting from an initial guess for the solution and the mesh, at each iteration the method adapts the mesh to obtain a sufficiently accurate numerical solution. The accuracy is measured by controlling the size of the residuals of numerical solution in both differential equations and boundary conditions.

The solution satisfying adhesion constraints is obtained by means of a numerical limit procedure for discrete values of the penalty parameters, as

$$\boldsymbol{y} = \lim_{k_r, k_{r\theta} \to \infty} \boldsymbol{y}_k. \tag{25}$$

It is worth noting that each element of the sequence generated by the penalty procedure is in turn the result of a non-linear iteration process needed to satisfy the non-linear differential problem (22). Moreover, it should be noted that crack growth is simulated solving the equilibrium problem Eq. (22) for a fixed crack length, namely for a fixed fracture function $d(\theta)$ equal to 1 along the cracked region and to zero in the uncracked one.

In the numerical calculations the same values have been adopted for the sliding and opening penalty parameters. The penalty procedure has been terminated until the numerical solution has satisfied the following tolerance criterion based on the energy release rates:

$$\max\{eG_{\mathrm{I}}, eG_{\mathrm{II}}, eG_{\mathrm{T}}\} \leqslant 10^{-3}, \tag{26}$$

where eG_{I}, eG_{II} and eG_{T} represent the relative errors for energy release rate mode components and total energy release rate, respectively. As an example, for the mode I component we have

$$eG_{\mathrm{I}} = \frac{|\, G_{\mathrm{I}}^{j} - G_{\mathrm{I}}^{j-1} \,|}{G_{\mathrm{I}}^{j}}, \tag{27}$$

where the superscript j refers to the actual values of penalty parameters whereas $j-1$ is referred to the previous one.

As a result of stress singularities at the crack tip arising when the stiffness parameters of the interface k_r and $k_{r\theta}$ tend to infinity, the solution can change very quickly approaching to a discontinuous behavior, thus requiring a very accurate integration which has been obtained through an appropriately fine mesh. A mesh point has been placed in correspondence of the crack tip in order to evaluate accurately the interface relative displacements appearing in Eq. (9). Moreover, for large values of the penalty parameters k_r and $k_{r\theta}$ a supposition good enough to represent the rapid change of the solution must be adopted. To this aim a continuation technique in the penalty parameters has been utilized, according to which the mesh and solution for one value of the penalty parameters is used as an initial supposition for larger values.

The proposed methodology can be extended to problems of interfacial crack growth between sublaminates with different mechanical properties and with arbitrary curvature. With reference to the former aspect, it has been shown that the use of beam or plate models, which eliminate deformations in the thickness direction, leads to avoid the non convergence behavior of individual energy release rates, a direct consequence of the classical oscillatory behavior of stress singularities predicted by the elasticity theory when delamination is placed between two different materials. In fact, the proposed methodology (plate or beam models + interface models) has been extended to analyze plane interface crack of arbitrary shape in laminated plates (see Bruno et al., 2005) also when oscillatory singularities may exist. In these cases it has been evidenced that individual energy release rates assume convergent and well defined values contrarily to the results obtained by using the continuum model and carried out by adopting solid finite elements. As far as interface cracks of arbitrary curvature are concerned, it should be noted that the proposed method should be extended by adopting a beam theory appropriate for a variable curvature radius, for each layer

kinematics. For instance, the specialization of the shell theory developed in (Reddy, 1982) could be adopted.

Moreover, multiple delaminations may be also simulated in the context of the proposed method by substituting the bare interface layer simulated by means of the Lagrangian multiplier technique, with cracking interface layers characterized by a constitutive law equal to that expressed in Eq. (8). Introducing the above cracking interface models leads to model the presence of further delaminations and to compute by means of Eq. (9) the energy release rates at the different interface crack tips for fixed values of crack lengths.

4.2. Curved beam with an internal interfacial crack

The problem of an isotropic and homogeneous curved beam with an off-set internal curved crack schematized in Fig. 3 is now analyzed. The beam has total thickness $H = h_1 + h_2$, internal and external radius of curvature R_i and R_o, respectively, and is subjected to bending moments at both ends. The thickness ratio of the beam h_1/h_2 is equal to 3 and E is the Young modulus. The curvature and bending loading condition produce both interlaminar tensile and shear stresses along the curved interface containing the crack. The combined action of the through the thickness stresses is responsible for mixed-mode interfacial crack growth. In order to study the problem an appropriate assembly of interface and beam elements must be used to capture interlaminar stresses with a good accuracy. Due to the symmetry only one-half of the model has been analyzed. At the symmetry plane $\theta = \pi/2$ (see Fig. 3), mid-axis horizontal displacements $\bar{u}_i$, rotations ψ_i and shear stress resultants T_i are imposed zero for each beam elements ($i = 1, \ldots, n_u + n_l$). In addition to these boundary conditions, in order to exclude possible rigid body motions along the vertical direction, an artificial constraint imposing nullity of the vertical displacement of the lowest beam element w_1, is applied.

To this end, the effect of the number of beam elements on the accuracy of the solution is investigated in Fig. 4, where results from the present analysis in terms of the dimensionless total energy release rate are plotted as a function of the half-crack angle $\theta_D/2$ for different beam element subdivisions (denoted as $(n_l - n_u)$). The radius ratio R_i/R_o is equal to 4/5. In the numerical calculations the following parameters have been adopted: $h_1 = 1.5$ mm $h_2 = 0.5$ mm, $E = 70{,}000$ N/mm^2. Both the case of constant (i.e. (1–1), (4–3)) and variable (i.e. (2–2)var, (4–3)var) beam thicknesses in each sub-laminate are considered in the model assembly. The thickness distributions in the (2–2)var, (4–3)var models are shown in Table 1. In addition in Fig. 4 results obtained in Lu et al. (1994) by using a classical FE model are plotted. It can be seen that the FE results for the total energy release rate versus crack length are in good agreement with the present model for all the beam assemblies. The relative errors $\Delta G/G_{FEM}$, with ΔG evaluated as the absolute

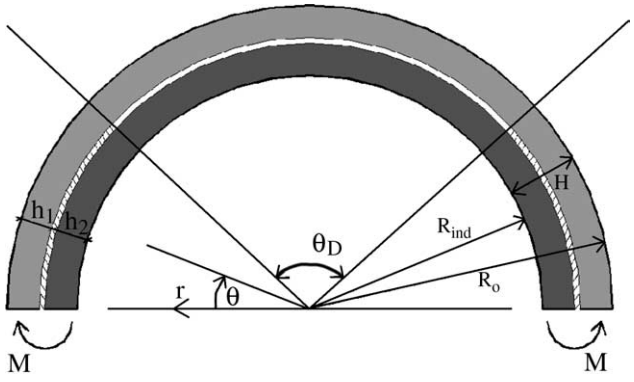

Fig. 3. Curved beam with an internal interfacial crack subjected to bending moments.

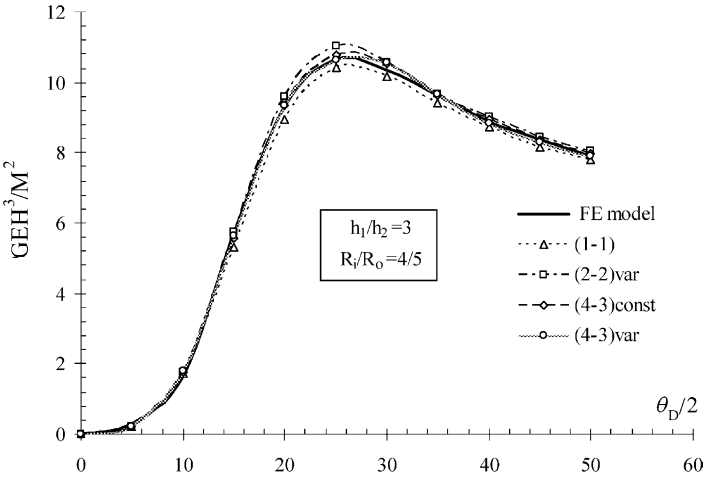

Fig. 4. Dimensionless total energy release rate for an isotropic curved beam in bending as a function of crack extension: influence of division in beam elements and comparison with the FE results of Lu et al. (1994).

Table 1
Thickness distribution for beam models with non-uniform thicknesses

Beam model ($n_l - n_u$)	t_i/h_1	t_i/h_2
(2–2)	0.867/0.133	0.4/0.6
(4–3)	0.4/0.4/0.1/0.1	0.3/0.3/0.4

value of the difference between the present model and the FE one, shown in Table 2 are within 8% except for very short crack lengths ($\theta_D/2 = 5°$) for which as expected the beam model is not appropriate, even if the relative errors decrease with an increasing number of beam elements. As a matter of fact for short crack lengths the curved laminated beam theory adopted to model each beam element is not appropriate, since the layers comprised in the cracked region become too thick and should be modeled by using the 2D continuum theory.

In addition in Table 2 the average error with respect to the considered crack lengths is shown. These values are somewhat misleading as to the accuracy of the model since results present an accuracy much better than 6% because much of the difference occurs for short crack lengths ($\theta_D/2 = 5°$, 10°). The models with the lower average relative errors are the (4–3)var and the (4–3) ones although for some crack lengths the (2–2) model may show the best accuracy. The (4–3)var and the (4–3) models, as a matter of fact, reflect more accurately the geometry of the component. Results for the (4–3)var and the (4–3) models are very similar.

Table 2
Relative errors for the total energy release rate for different crack lengths. $R_i/R_o = 4/5$

$\Delta G/G_{FEM}$											Average
($n_u - n_l$)	$\theta_D/2 = 5°$	$\theta_D/2 = 10°$	$\theta_D/2 = 15°$	$\theta_D/2 = 20°$	$\theta_D/2 = 25°$	$\theta_D/2 = 30°$	$\theta_D/2 = 35°$	$\theta_D/2 = 40°$	$\theta_D/2 = 45°$	$\theta_D/2 = 50°$	
(1–1)	0.3405	0.0365	0.0680	0.0378	0.0216	0.0180	0.0197	0.0172	0.0250	0.0134	0.0598
(2–2)var	0.2900	0.0719	0.0048	0.0322	0.0342	0.0205	0.0062	0.0155	0.0086	0.0148	0.0499
(4–3)const	0.2832	0.0712	0.0238	0.0046	0.0134	0.0152	0.0028	0.0061	0.0003	0.0090	0.0430
(4–3)var	0.2991	0.0825	0.0105	0.0039	0.0013	0.0185	0.0052	0.0041	0.0081	0.0030	0.0436

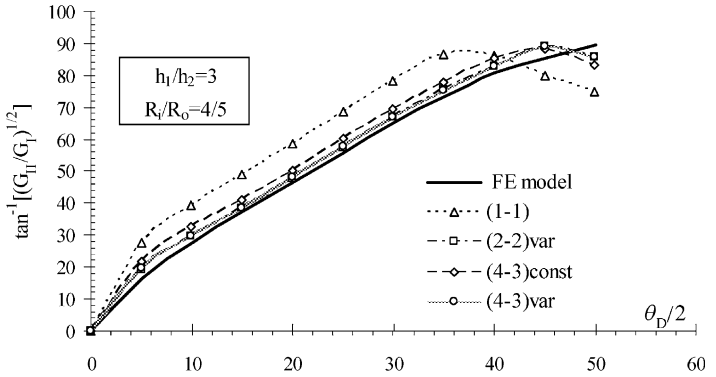

Fig. 5. Mode mix ratio for an isotropic curved beam in bending as a function of crack extension: influence of beam element subdivision and comparison with the FE results of Lu et al. (1994).

Therefore, with respect to the total energy release rate, the simplest (1–1) model adopting one beam element for each sub-laminate is sufficient to predict the total energy release rate with a reasonable accuracy. On the contrary the use of the classical curved beam theory leads to a reproduction of only limiting cases of the solution, such as the steady state behavior for longer cracks, and loses accuracy for thicker configurations as shown in Lu et al. (1994).

On the other hand, the situation changes notably in terms of mode partition since more than one beam element must be adopted into each sub-laminate in order to capture the mode mix ratio, as shown in Fig. 5. The mode mix ratio is expressed by the phase angle $\psi = \tan^{-1}[(G_{II}/G_I)^{1/2}]$. The models with lower average errors are those with the (2–2)var and the (4–3)var subdivisions, with errors within 8% except for $\theta_D/2 = 5°$. This is shown in Table 3 where the relative errors $\Delta\psi/\psi_{FEM}$, with $\Delta\psi$ evaluated as the absolute value of the difference between the present model and the FE one, are illustrated. The worst results are obtained for very short crack lengths ($\theta_D/2 = 5°$) with errors within about 17% for the (2–2)var model. For the limit case of $\theta_D \to 0°$ the crack is approximately in pure mode I, as in the case of a crack in a infinite body loaded by tensile stresses, therefore the phase angle has been considered to be zero in the plot. As shown in Fig. 5 the crack tend to close since a pure mode II condition is reached for crack lengths with angles θ_D larger than 100°. As a consequence, results out of this range are not plotted. As expected the use of only one beam element for each sublaminate is not appropriate since the 2D nature of the mode mix problem cannot be captured. The solution, however, converges rapidly to the FE one as the number of beam elements increases as shown in Fig. 6.

The case of a thicker curved beam configuration with a radius ratio R_i/R_o equal to 2/3 and a thickness ratio h_1/h_2 equal to 3, is also considered in Figs. 7–9. In the numerical calculations the following parameters have been adopted: $h_1 = 3$ mm, $h_2 = 1$ mm, $E = 70{,}000$ N/mm^2. In general results are somewhat worse than in the thinner case since the effects of shear are more prevalent on the solution and a more accurate beam

Table 3
Relative errors for the mode mix ratio as a function of crack lengths. $R_i/R_o = 4/5$

$\Delta\psi/\psi_{FEM}$											Average
$(n_u - n_l)$	$\theta_D/2 = 5°$	$\theta_D/2 = 10°$	$\theta_D/2 = 15°$	$\theta_D/2 = 20°$	$\theta_D/2 = 25°$	$\theta_D/2 = 30°$	$\theta_D/2 = 35°$	$\theta_D/2 = 40°$	$\theta_D/2 = 45°$	$\theta_D/2 = 50°$	
(1–1)	0.690	0.417	0.321	0.258	0.235	0.196	0.185	0.067	0.062	0.166	0.260
(2–2)var	0.175	0.078	0.036	0.026	0.035	0.027	0.034	0.027	0.047	0.044	0.053
(4–3)const	0.336	0.169	0.105	0.081	0.082	0.065	0.066	0.059	0.037	0.074	0.107
(4–3)var	0.216	0.074	0.038	0.028	0.037	0.023	0.031	0.028	0.046	0.044	0.057

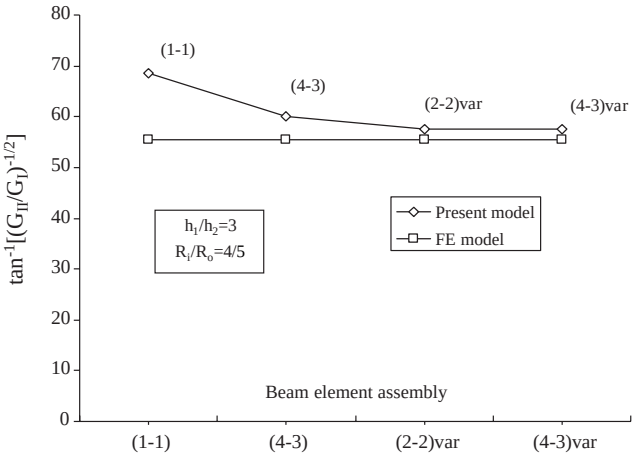

Fig. 6. Convergence to finite element results by increasing the number of beam elements in the assembly for a crack angle $\theta = 25°$.

Table 4
Relative errors for the total energy release rate for different crack lengths. $R_i/R_o = 2/3$

$\Delta G/G_{FEM}$										Average
$(n_u - n_l)$	$\theta_D/2 = 10°$	$\theta_D/2 = 15°$	$\theta_D/2 = 20°$	$\theta_D/2 = 25°$	$\theta_D/2 = 30°$	$\theta_D/2 = 35°$	$\theta_D/2 = 40°$	$\theta_D/2 = 45°$	$\theta_D/2 = 50°$	
(1–1)	0.3812	0.2062	0.1238	0.0864	0.0650	0.0602	0.0568	0.0614	0.0537	0.1216
(2–2)const	0.3913	0.2090	0.1133	0.0562	0.0237	0.0122	0.0139	0.0142	0.0094	0.0937
(2–2)var	0.3504	0.1462	0.0496	0.0108	0.0150	0.0142	0.0122	0.0058	0.0068	0.0679
(4–3)var	0.3572	0.1591	0.0636	0.0550	0.0156	0.0051	0.0222	0.0237	0.0317	0.0815

Table 5
Relative errors for the mode mix ratio as a function of crack lengths. $R_i/R_o = 2/3$

$\Delta\psi/\psi_{FEM}$										Average
$(n_u - n_l)$	$\theta_D/2 = 10°$	$\theta_D/2 = 15°$	$\theta_D/2 = 20°$	$\theta_D/2 = 25°$	$\theta_D/2 = 30°$	$\theta_D/2 = 35°$	$\theta_D/2 = 40°$	$\theta_D/2 = 45°$	$\theta_D/2 = 50°$	
(1–1)	0.586	0.435	0.373	0.316	0.273	0.255	0.223	0.210	0.094	0.277
(2–2)const	0.309	0.206	0.173	0.140	0.119	0.116	0.098	0.096	0.102	0.136
(2–2)var	0.121	0.059	0.057	0.042	0.033	0.039	0.032	0.037	0.045	0.047
(4–3)var	0.152	0.069	0.058	0.045	0.034	0.040	0.032	0.034	0.045	0.051

model is required (see Tables 4 and 5). However, the general trend of the solution is similar to the thinner case. As a matter of fact, the models with lower average errors are those with the (2–2)var and the (4–3)var subdivisions. With reference to the (2–2)var model the errors for the total energy release rate are within 5% except for $\theta_D/2$ less or equal than 15°, whereas for the mode partition within 6% except for $\theta_D/2$ less or equal than 10°. The worst results are obtained for very short crack lengths. As shown in Fig. 8 the crack tends to close since a pure mode II condition is reached for crack lengths with angles θ_D larger than 130°. As a consequence, results out of this range are not plotted. The convergence of the solution as the number of beam elements increases is investigated in Fig. 9.

For the brevity results obtained for different positions of the crack along the thickness are not presented here, but they appeared very similar to the previous discussed situations. The additional calculations have shown that the accuracy is better when the crack is at the beam mid-axis.

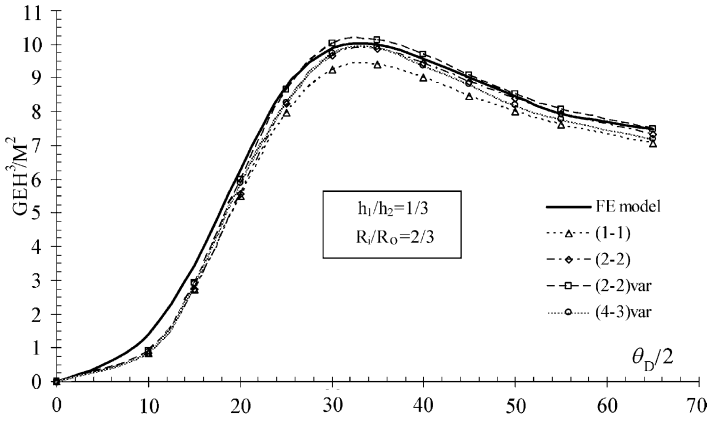

Fig. 7. Dimensionless total energy release rate for an isotropic curved beam in bending as a function of crack extension: influence of beam element subdivision and comparison with the FE results of Lu et al. (1994).

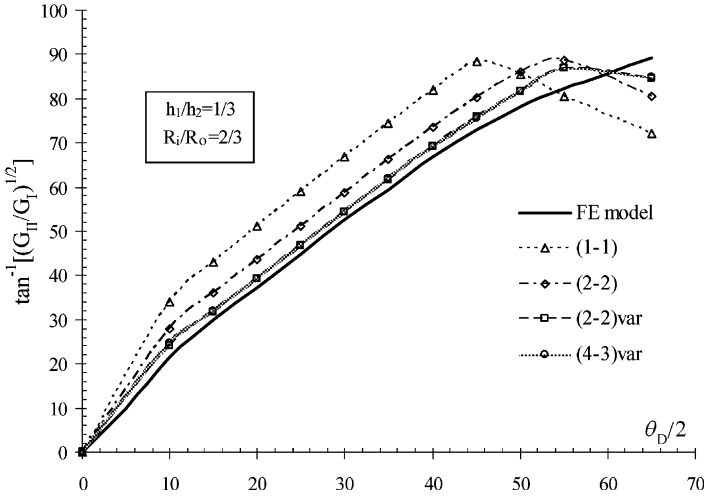

Fig. 8. Mode mix ratio for an isotropic curved beam in bending as a function of crack extension: influence of beam element subdivision and comparison with the FE results of Lu et al. (1994).

4.3. Curved beam with an edge interfacial crack

The example of a curved beam with an edge crack is now considered. The beam is clamped at one end and is loaded on the cracked sub-laminates at the other one. The geometrical configuration of the beam is shown in Fig. 10.

4.3.1. Influence of the curvature: transverse and axial end forces

At first the influence of curvature on the energy release rates is investigated by considering a specimen with a constant length of the lower surface L and lower thickness h_1 and varying the radius of curvature in such a way to obtain a variation for θ_T from 0 to π.

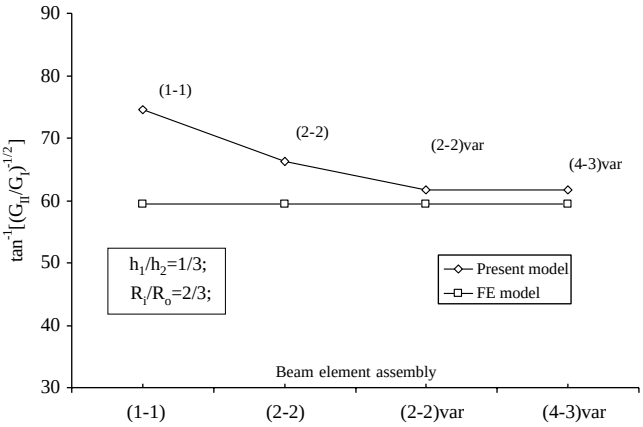

Fig. 9. Convergence to finite element results by increasing the number of beam elements in the assembly for a crack angle $\theta_D/2 = 35°$.

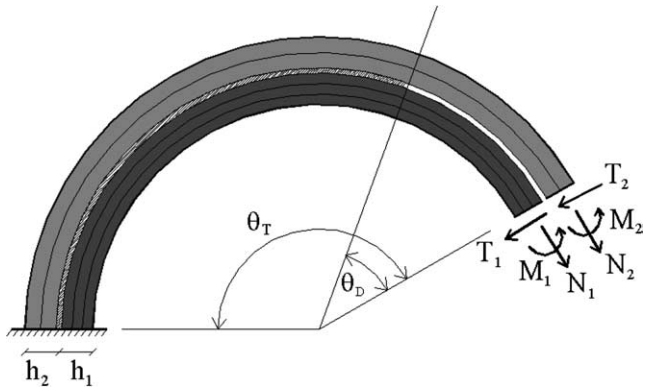

Fig. 10. Geometrical and loading configurations of the curved beam with and edge delamination.

In the tests the angle subtended by the delamination θ_D is taken to be 1/3 of the total angle θ_T.

Different thickness ratios h_2/h_1 have been considered in the calculations. The lower thickness is assumed equal to 1 mm, and the length of lower surface beam 30*mm*. The beam models (1–1), (2–2) and (4–3) with a uniform beam element subdivision are used in the calculations.

Figs. 11 and 12 show the variation of the total energy release rate and of its individual mode components with respect to the beam curvature h_1/R_i, respectively, in the case of two opening loads normal to the beam axis, i.e. $T_1 = -T_2$. The beam is made of an isotropic homogeneous material with the same characteristics of the previous example. Results plotted in Fig. 11 show that the total energy release rate decreases as the curvature increases, especially when the crack is moved toward the upper surface of the beam, pointing out that curvature is a restrictive cause for crack growth when transverse loads are applied. This result is in agreement with (Münch and Ousset, 2002). Calculations carried out by using different beam element subdivisions have shown that the total energy release rate is practically unaffected by the number of beam elements introduced into each sublaminate and is well captured also when a rough subdivision, namely the (1–1) model, is adopted. Only a small underestimation is provided if beam models rougher than the (4–3) one are adopted. On the contrary the mode partition is strictly affected by the adopted number of beam elements. Consequently, in Fig. 12 only results for the (4–3) model are plotted showing that for a crack

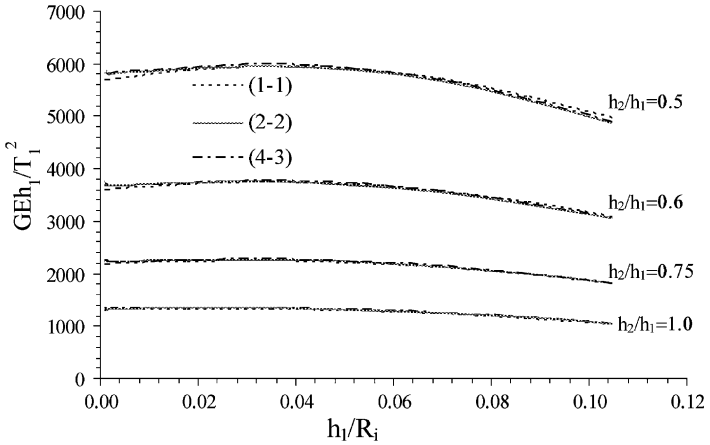

Fig. 11. Dimensionless total energy release rate as a function of the curvature for two end opposite transverse forces.

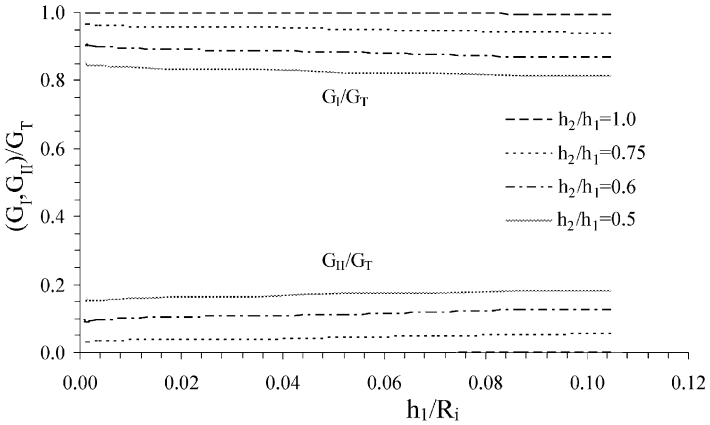

Fig. 12. Relative amounts of mode components as a function of the curvature for two end opposite transverse forces.

aligned with the beam axis a pure mode I condition is reached, whereas as the crack moves toward the upper surface of the beam the relative amount of mode I decreases. Finally, it can be seen that the relative amount of mode I decreases whereas the relative amount of mode II increases slowly for an increasing curvature.

The case of two opposite axial forces, i.e. $N_1 = -N_2$, is considered in Figs. 13 and 14, where the situation is contrary to the previous case of transverse forces, since curvature is an encouraging factor for crack growth. In Fig. 13 results refer to the (1–1), (2–2) and (4–3) beam assemblies, whereas in Fig. 14 only the (4–3) beam model is considered. As a matter of fact, the total energy release rate is an increasing function of h_1/R_i, since a geometrical coupling between shear, bending and axial deformability effects arises in proximity of the crack tip when the curvature increases. Moreover this effect is more evident when the crack moves away from the beam axis. This aspect is also pointed out by the mode partition behavior as a function of the curvature shown in Fig. 14: here it can be seen that the fracture mode I becomes prevalent for large values of the curvature, whereas for small values fracture mode II condition prevails. In fact, bending and shear deformability effects, which are prevalent for large curvatures, activate the mode I energy release rate component, whereas axial deformability, which prevails for small curvatures, is responsible mainly for mode II energy release rate.

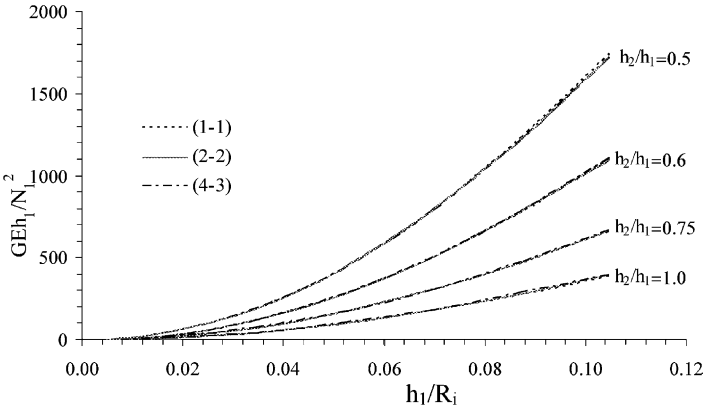

Fig. 13. Dimensionless total energy release rate as a function of the curvature for two opposite axial forces.

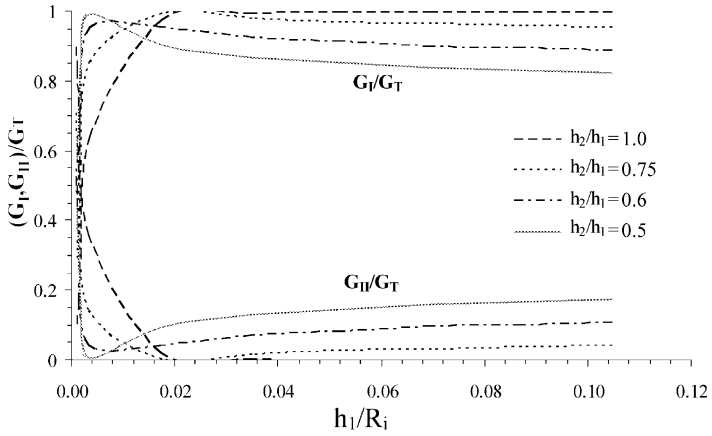

Fig. 14. Relative amounts of mode components as a function of the curvature for two opposite axial forces.

4.3.2. Comparisons with FE results

To assess the reliability of analysis for the edge cracked curved beam a classical FE model has been built. The curved beam has been modeled by using 8-noded using 2D plane stress finite elements and energy release rates have been calculated by using the virtual crack closure technique (Rybicki and Kanninen, 1977) in terms of nodal forces and displacements. The FEM model is presented in Fig. 17. A sufficiently dense mesh has been adopted in order to capture the large stress gradient at the crack tip. A constant size for finite elements has been assumed in the circumferential direction along the beam in order to study the delamination growth. Moreover, the size of finite elements has been chosen uniform through the thickness. The crack interface has been modeled by two translational spring elements in the radial and circumferential directions with high stiffness released to simulate interlaminar cracking. Nodal forces necessary to apply the virtual crack closure procedure are obtained from the reactions of the springs. A variable number of finite elements in the circumferential direction and in the radial direction has been adopted in order to perform convergence studies for the total and individual energy release rates. To establish the optimal dimensions of the mesh discretisation Δ_θ and Δ_r (see Fig. 17), element sizes have been varied from $\Delta_\theta/h_1 = 0.25$ to $\Delta_\theta/h_1 = 0.025$, whereas the maximum Δ_r/Δ_θ ratio has been 2. For computational convenience the lower sublaminate the radial size of the finite element mesh is assumed twice that of the upper one. These results have

shown that a circumferential element size equal to $\Delta_\theta/h_1 = 0.0375$, is sufficient to obtain converged values for the total and individual energy release rates and therefore has been adopted for numerical computations.

The results of computational studies for the case of two edge opposite transverse forces (i.e. $T_1 = -T_2$) are shown in Figs. 15 and 16 for an isotropic and a cylindrical orthotropic but homogeneous material with a longitudinal-to-transverse shear modulus ratio E_x/G_{xy} equal to 100, respectively, where both the total and individual energy release rates are plotted as a function of the thickness ratio h_2/h_1. The total angle subtended by the beam is $\theta_T = \pi$ and the other parameters are the same of the previous examples. The curves for the energy release rates show a decreasing behavior due to the increase of beam stiffness as the thickness ratio increases. Moreover, it can be seen the total energy release rate from the FE model is well estimated also if a small number of beam elements is adopted, whereas individual mode components are reasonably

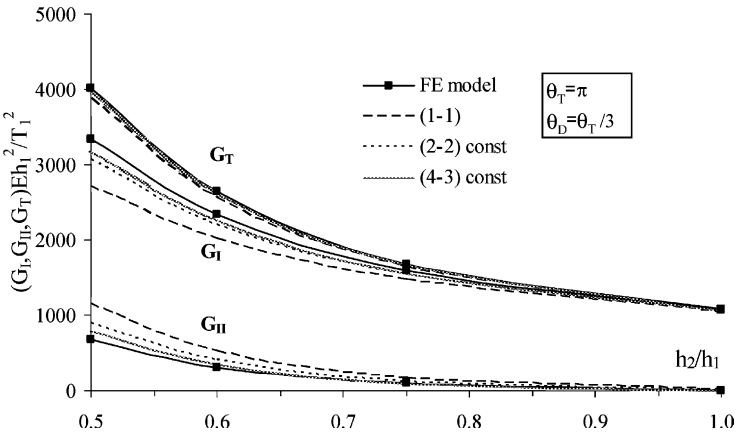

Fig. 15. Energy release rates as a function of the thickness ratio h_2/h_1 for an isotropic beam loaded by two opposite transverse forces: comparison with 2D FE results.

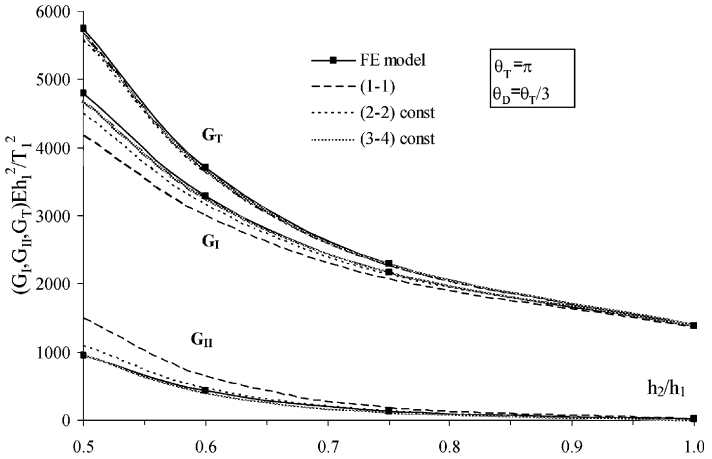

Fig. 16. Energy release rates as a function of the thickness ratio h_2/h_1 for a cylindrical orthotropic beam ($E_x/G_{xy} = 100$) loaded by two opposite transverse forces: comparison with 2D FE results.

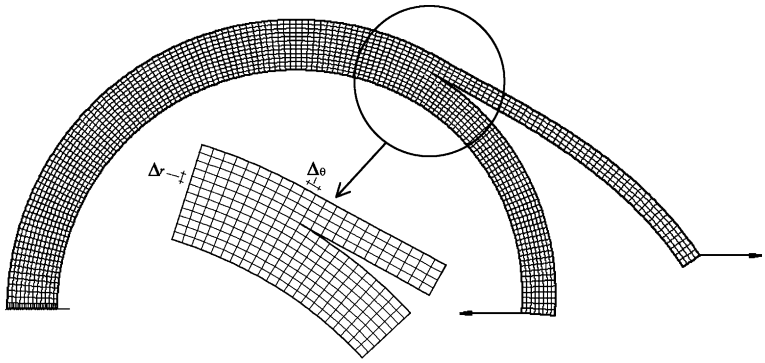

Fig. 17. FEM model of the curved beam used for comparisons with results of the present approach.

captured only if an accurate beam model is adopted. In fact, except when h_2 is near to h_1 and a pure mode I condition is practically attained, beam models (1–1) and (2–2) may lead to large discrepancies in comparison with the FE results especially for small thickness ratios (for instance the (1–1) model provides a relative error with respect to FE results of about 19% for $h_2/h_1 = 0.50$ for the isotropic beam with respect to the mode I energy release rate component). On the contrary the mode I energy release rate when the (4–3) beam model is used, has an accuracy better than 3% both for the isotropic and the orthotropic cases as shown in Table 6 where the absolute relative errors for the total and individual energy release rates with respect to the FE results are shown for different thickness ratios. Each value in the Table presents the absolute difference between the current method and the FE results divided by the FE result. The errors shown in the table for the mode II energy release rate component appear notable especially for large thickness ratios because G_{II} is very small for these configurations and thus are confusing as to the global accuracy of the method. The trends of the isotropic and orthotropic cases are similar but, as expected, the orthotropic case shows larger values of the energy release rates with respect to the isotropic case due to its larger deformability (for instance the increment of energy release rates is about 18% when $h_2/h_1 = 0.5$).

Finally, Fig. 18 shows the behavior of the energy release rates as the interlaminar crack grows for the isotropic case and a fixed thickness ratio $h_2/h_1 = 0.5$. As the interlaminar crack grows from the loaded edge towards the other one to the energy release rates increase rapidly and reach a maximum at about $\theta_D = \pi/2$ and then decreases in a quasi-symmetric way. As a matter of fact, bending moments and axial forces at the crack tip are equal for symmetrical crack configurations, namely for θ_D and $\pi - \theta_D$, whereas shear forces are opening for $0 < \theta_D < \pi/2$ and closing for $\pi/2 < \theta_D < \pi$. This causes a small reduction of the total and mode I energy release rates for angles larger than $\pi/2$ and produces a closure of the crack for angles near π. On the contrary the mode II energy release rate shows a relatively small increment. Therefore, a crack growth criterion based on the total energy release rate is adopted, exhibit an unstable behavior for angles

Table 6
Relative errors for total and individual energy release rates obtained from the (4–3) multi-layer model with respect to the FE model for the isotropic and orthotropic beams

h_2/h_1	Orthotropic			Isotropic		
	$\Delta G_T/G_T$(FE)	$\Delta G_I/G_I$(FE)	$\Delta G_{II}/G_{II}$(FE)	$\Delta G_T/G_T$(FE)	$\Delta G_I/G_I$(FE)	$\Delta G_{II}/G_{II}$(FE)
0.50	0.017	0.025	0.019	0.001	0.023	0.126
0.60	0.011	0.007	0.040	0.002	0.022	0.148
0.75	0.003	0.007	0.174	0.008	0.013	0.091
1.00	0.014	0.021	0.794	0.006	0.004	0.466

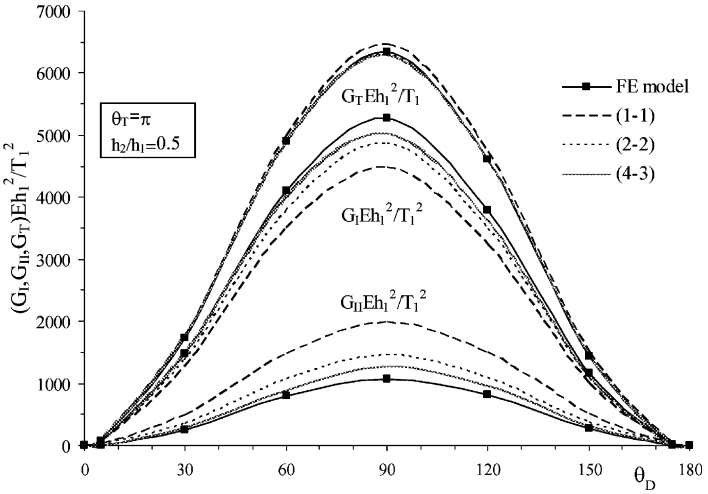

Fig. 18. Total energy release rate and mode components predicted by the FE model and the present approach as the crack grows for the isotropic beam loaded by two opposite transverse forces.

θ_D between 0 and $\pi/2$, and a stable one for larger values. This however corresponds to a rough approximation of the fracture criterion and generally more accurate mode-mix dependent fracture criterion should be adopted. From comparisons with FE results in Fig. 18 it can be concluded that the present approach does quite well for both the total and individual energy release rate components when the (4–3) assembly is adopted. Moreover, the results show that the mode partition converges to the FE values as the number of beam elements increases.

5. Conclusions

An efficient method has been presented for the prediction of mixed mode interfacial crack growth in circular layered beams based on a multi-layer beam kinematics and on interface modeling. The curved beam is simulated by a sequence of curved layers connected by interfaces, modeled as a zero thickness layers. A first order shear deformable curved beam theory is adopted for each layer. The interface containing the crack simulates the presence of an interfacial crack by means of a cracking constitutive law and ensures displacement continuity between layers in the uncracked regions by means of the penalty method. Adhesion between perfectly bonded beam layers is imposed by means of interfaces which implement the Lagrangian multipliers method. The use of the two constraint methods, namely, the penalty and Lagrange multipliers methods, incorporated into the interface models leads to an improvement of the efficiency of the approach. The analysis is carried out through the solution of an accurate numerical integration scheme, the boundary value problem obtained by means of a variational formulation. Results have been obtained for circular beams with edge and internal cracks in order to show the influence of shear deformation and of curvature. Both the case of a homogeneous isotropic and cylindrical orthotropic materials have been considered.

Numerical calculations carried out by this approach have shown a good correlation with results obtained by using the 2D finite element method and the virtual crack closure technique both for the total and the individual mode components of energy release rate for all loading cases and geometrical configurations considered. These comparisons with very accurate FE solutions assess the validity of the proposed model to describe the mixed-mode crack circular beam problem. In particular, the total energy release rate is well approached even with a two-layer beam model whereas more than one beam model is needed into each

sub-laminate to capture the mode partition with a sufficient accuracy. The mode partition predicted by the present method approaches to the FE results if the beam model is improved by introducing an increasing number of interface and beam elements. However, an approximation to the mode partition problem acceptable from the engineering point of view can be obtained even with a rough beam element assembly by choosing an appropriate subdivision which reflect the physical configuration of the curved beam. The proposed method, in spite of its simplicity, has shown its ability to provide a complete description of the mixed-mode interfacial crack problem for circular beams, which accounts for shear deformability and curvature effects. The numerical studies have shown that the curvature may have both a restrictive and encouraging effect on interfacial crack growth. As a matter of fact for the central cracked beam in bending and for the edge cracked beam subjected to transverse forces the total and the mode I energy release rate decrease as the curvature increases, whereas in the case of axial forces for the edge cracked beam the total and individual energy release rates increases. Moreover, shear deformability is advantageous for interfacial cracking since it has been verified that when the transverse shear modulus diminishes the energy release rates increases for the edge cracked beam subjected to transverse forces.

References

Allix, O., Corigliano, A., 1999. Geometrical and interfacial non-linearities in the analysis of delamination in composites. International Journal of Solids and Structures 36, 2189–2216.

Baldacci, R., 1983. Scienza delle Costruzioni, vol. 2. UTET, Torino, Italy (in Italian).

Bruno, D., Greco, F., Lonetti, P., 2003. A coupled Interface-multilayer approach for mixed mode delamination and contact analysis in laminated composites. International Journal of Solids and Structures 40, 7245–7268.

Bruno, D., Greco, F., 2001. Mixed mode delamination in plates: A refined approach. Internatioal Journal of Solids and Structures 38 (50–51), 9149–9177.

Bruno, D., Greco, F., Lonetti, P., 2005. A delamination modelling technique based on plate and interface theories for 3d laminated structures. European Journal of Mechanics A/Solids 24, 127–149.

Camanho, P.P., Dávila, C.G., Moura M.F, 2003. Numerical simulation of mixed-mode progressive delamination in composite materials. Journal of Composite Materials 37 (16), 1415–1438.

Cox, B.N., Massabò, R., Kedward, K., 1996. Suppression of delaminations in curved structures by stitching. Composites Part A 27A, 1133–1138.

Cui, W., Liu, T., Len, J., Ruo, R., 1996. Interlaminar tensile strength (ILTS) measurement of woven glass/polyester laminates using four-point curved beam specimen. Composites Part A 27A, 1097–1115.

Figiel, L., Kamiński, M., 2003. Mechanical and thermal fatigue delamination of curved layered composites. Computers and Structures 81, 1865–1873.

Hutchinson, J.W., Suo, Z., 1992. Mixed mode cracking in layered materials. In: Hutchinson, J.W., Theodore, Y.W. (Eds.), Advances in Applied Mechanics, vol. 28. Academic Press, New York, pp. 63–191.

Jones, R.M., 1975. Mechanics of Composite Materials. Scripta, Washington, DC.

Kaczmarek, K., Wisnom, M.R., Jones, M.I., 1998. Edge delamination in curved $(0_4/\pm 45_6)$s glass-fibre/epoxy beams loaded in bending. Composite Science and Technology 58, 155–161.

Kedward, K.T., Wilson, R.S., McLean, S.K., 1989. Flexure of simply curved composites shapes. Composites 20, 365–398.

Lekhnitskii, S.G., Tsai, S.W., Cheron, T., 1968. Anisotropic Plates. Gordon and Breach Science Publishers, New York.

Lu, T.J., Xia, Z.C., Hutchinson, J.W., 1994. Delamination of beams under transverse shear and bending. Materials Science and Engineering A 188, 103–112.

McRobbie, S., Longmuir, A.J., Wilcox, J., Gibson, A.G., Chandler, H.W., 1995. Through the thickness stress in curved laminates of single- and double-skinned construction. Composites 26, 339–345.

Münch, A., Ousset, Y., 2002. Numerical simulation of delamination growth in curved interfaces. Computer Methods and Applied Mechanics Engineering 191, 2045–2067.

Raju, I.S., 1987. Calculation of strain-energy release rates with higher order and singular finite elements. Engineering and Fracture Mechanics 28, 251–274.

Reddy, J.N., 1982. Analysis of layered composite plates accounting for large deflection and transverse shear strains. In: Hinton, E., Owen, D.R.J., Taylor, C. (Eds.), Recent Advances in Non-linear Computational Mechanics. Pineridge Press, Swansea, UK, pp. 155–202.

Reeder, J.R., 1993. A Bilinear Failure Criterion for Mixed-mode Delamination. in Composite Materials: Testing and Design, vol. 11. ASTM STP 1206: American Society for Testing and Materials, pp. 303–322.

Rybicki, E.F., Kanninen, M.F., 1977. A finite element calculation of stress intensity factors by a modified crack closure integral. Engineering and Fracture Mechanics 9, 931–938.

The MathWorks Inc., 2000. Using MATLAB®, Version 6, 3 Apple Hill Drive, Natick, MA.

Timoshenko, S., 1934. Theory of Elasticity. McGraw-Hill Book Company, New York and London.

Wang, J., Qiao, P., 2004a. Interface crack between two shear deformable elastic layers. Journal of the Mechanics and Physics of Solids 52, 891–905.

Wang, J., Qiao, P., 2004b. On the energy release rate and mode mix of delaminated shear deformable composite plates. International Journal of Solids and Structures 41, 2757–2779.

Wisnom, M.R., Jones, M.I., 1995. Delamination due to interaction between curvature induced interlaminar tension and stresses at terminating plies. Composite Structures 32, 615–620.

Zou, Z., Reid, S.R., Li, S., Soden, P.D., 2002. Application of a delamination model to laminated composite structures. Composite Structures 56, 375–389.

Zou, Z., Reid, S.R., Li, S., 2003. A continuum damage model for delaminations in laminated composites. Journal of the Mechanics and Physics of Solids 51, 333–356.

Zou, Z., Reid, S.R., Soden, P.D., Li, S., 2001. Mode separation of energy release rate for delamination in composite laminated using sublaminates. International Journal of Solids and Structures 38, 2597–2613.